ARTICLE

A Novel Meshfree Analysis of Transient Heat Conduction Problems Using RRKPM

Hongfen Gao[1] and Gaofeng Wei[2,3,*]

[1]College of Intelligent Engineering, Shandong Management University, Jinan, 250357, China

[2]School of Mechanical and Automotive Engineering, Qilu University of Technology (Shandong Academy of Sciences), Jinan, 250353, China

[3]Shandong Institute of Mechanical Design and Research, Jinan, 250353, China

[*]Corresponding Author: Gaofeng Wei. Email: wgf@qlu.edu.cn

ABSTRACT

By introducing the radial basis functions (RBFs) into the reproducing kernel particle method (RKPM), the calculating accuracy and stability of the RKPM can be improved, and a novel meshfree method of the radial basis RKPM (meshfree RRKPM) is proposed. Meanwhile, the meshfree RRKPM is applied to transient heat conduction problems (THCP), and the corresponding equations of the meshfree RRKPM for the THCP are derived. The two-point time difference scheme is selected to discretize the time of the THCP. Finally, the numerical results illustrate the effectiveness of the meshfree RRKPM for the THCP.

KEYWORDS

Transient heat conduction; meshfree method; reproducing kernel particle method; meshfree RRKPM; two-point difference method

1 Introduction

Many practical engineering structures run in high temperature, such as steam turbines, high-speed diesel engines and nuclear power plants, etc. The temperature field can change the properties of material structure. Therefore, it is an important subject to study the THCP of the structure in the condition of being heated [1,2].

Numerical simulation is an important analysis tool to research the THCP [3]. Finite element method (FEM) is one of the main numerical simulation methods. Many complex and difficult mechanical problems can be solved by the FEM, and valuable results can be derived [4,5]. However, due to the limitation of the correlation conditions between elements in the FEM, it is difficult to deal with the discontinuous problem in practical engineering problems, such as the formation of cracks and their mechanical behavior, the discontinuity in jointed rock mass and the crack propagation with moving boundary [6,7]. In order to improve the restriction of correlation conditions between elements, many novel methods have been proposed in recent years,

such as meshfree (or meshless, element-free) method [8,9], numerical manifold method (NMM) [10–12], boundary element method (BEM) [13,14], and numerical method based on least square method [15–17], etc.

The meshfree approximating technique is adopted in the meshfree method, which makes the approximating function free from the constraints of elements and greatly simplifies the analysis and calculation of pretreatment and crack propagation. Meshfree method has attracted attention in mechanics and practical engineering, and been widely used in the study of the THCP. At present, many meshfree methods have been developed, such as smooth particle hydrodymics (Abbreviation: SPH, proposed by Lucyt and Gingold in 1977) [18,19], element-free Galerkin method (Abbreviation: EFGM, proposed by Belytschko in 1994) [20–22], meshfree local Petrov-Galerkin method (Abbreviation: MLPG, proposed by Atluri in 1998) [23–26], reproducing kernel particle method (Abbreviation: RKPM, proposed by Liu in 2005) [27–30], radial basis functions method (Abbreviation: RBF, proposed by Žilinskas in 2010) [31,32], complex variable meshfree manifold method (Abbreviation: CVMMM, proposed by Gao in 2010) [33], the finite point method (Abbreviation: FPM, proposed by Tatari in 2011) [34,35], Hermit-type reproducing kernel particle method (Abbreviation: Hermit-type RKPM, proposed by Ma in 2017) [36–39] and boundary integral equation method (Abbreviation: BIE, proposed by Mantegh in 2010) [40,41], etc.

Because of the advantages of simple form and fast calculation speed, the RKPM is one of the meshfree methods which are widely applied and researched [42–44]. The RKPM is first proposed based on the SPH and the integral reconstruction theory of functions. The RKPM solves the boundary inconsistency, and eliminates the tensile instability of the SPH method. The method has some advantages, such as variable time frequency characteristics and multi-resolution characteristics. Therefore, the RKPM has been widely used in many practical engineering problems, such as large deformation analysis problems, structural dynamics problems, micro-electromechanical system analysis problems, nonlinear problem of hyperelastic rubber materials, high-speed impact problems and so on [45–47].

However, different kernel functions have different effects on the calculating accuracy and computational stability in the analysis of solving the THCP. In order to improve the calculating accuracy and stability of the RKPM, the RBF is introduced into the RKPM, and the meshfree RRKPM is proposed in this paper. Meanwhile, the meshfree RRKPM is applied to the THCP, and the corresponding equations of the meshfree RRKPM for THCP are derived. The numerical results illustrated the effectiveness of the meshfree RRKPM for the THCP.

2 Construction of the Approximating Function of Meshfree RRKPM

The approximating function $u^h(z)$ of Meshfree RRKPM can be written as a combination of the RKPM constructed by n nodes in the local problem domain and the RBFs constructed by m terms.

$$u^h(z) = \sum_{j=1}^{n} S_j^n(z)c_j + \sum_{i=1}^{m} S_i^m(z)a_i, \qquad z = (x, y)^T \tag{1}$$

where c_j and a_i represent the undetermined coefficients, n represents the number of the local influence domain, m represents the number of RBFs, S_i^m and S_j^n represent the RBFs and the reproducing kernel function (RKF), respectively.

The RBF S_i^m is the function of the distance r_i from calculating point z to the node z_i, $r_i = ||z - z_i||$

$$S_i^m(z) = (1 - \frac{r_i}{\delta})^6 (3 + 18\frac{r_i}{\delta} + 35\frac{r_i^2}{\delta^2}) \tag{2}$$

with δ denoting the scaling parameter.

The RKF S_j^n can be expressed as

$$S_j^n(z) = C(z, z_j)w(z - z_j)S_j^n(z_j)\Delta V_j \tag{3}$$

where $S_j^n(z_j)$ is the parameter of node z_j, ΔV_j is the area or volume of domain of influence, w is kernel function.

$$C(z, z_j) = \boldsymbol{b}^T(z)\boldsymbol{p}(z - z_j) \tag{4}$$

The coefficient matrix $\boldsymbol{b}(z)$ can be given by

$$\boldsymbol{b}(z) = [\, b_1(z), \, b_2(z), \, \cdots, \, b_n(z)\,]^T \tag{5}$$

The polynomial basis function $\boldsymbol{p}(z - z_j)$ is expressed as

$$\boldsymbol{p}^T(z - z_j) = [\, 1, \, x - x_j, \, y - y_j, \, (x - x_j)^2, \, (x - x_j)(y - y_j), \, (y - y_j)^2, \, \cdots\,] \tag{6}$$

The Eq. (1) can be rewritten as the following form:

$$u^h(z) = \sum_{j=1}^n S_j^n(z)c_j + \sum_{i=1}^m S_i^m(z)a_i = \sum_{I=1}^M S_I(z)a_I(z) = \boldsymbol{S}(z)\boldsymbol{a}(z) \quad (M = m + n) \tag{7}$$

in which $S_I(z)$ is basis function, $a_I(z)$ is corresponding coefficient, given by

$$\boldsymbol{S}(z) = [S_1^m(z), \, \cdots, \, S_m^m(z), \, S_1^n(z), \, \cdots, \, S_n^n(z)] \tag{8}$$

$$\boldsymbol{a}(z) = [a_1, \, \cdots, \, a_m, \, c_1, \, \cdots, \, c_n]^T \tag{9}$$

The approximating function $u^h(z)$ can be locally approximated in the neighborhood of calculating point z

$$u^h(z, \bar{z}) = \sum_{I=1}^M S_I(\bar{z})a_I(z) = \boldsymbol{S}(\bar{z})\boldsymbol{a}(z) \tag{10}$$

in which $\bar{z}$ is point of the neighborhood in calculating point z.

The weighted least squares method is used to obtain approximating functions $u^h(z)$ accurately in this paper. The weighted least squares function J is defined as

$$\begin{aligned} J &= \sum_{K=1}^N w(z - z_K)[u^h(z, z_K) - u(z_K)]^2 \\ &= \sum_{K=1}^N w(z - z_K)\left[\sum_{I=1}^M S_I(z_K)a_I(z) - u(z_K)\right]^2 \end{aligned} \tag{11}$$

where $w(z - z_K)$ is weighted function in the domain of influence, $z_K(K = 1, 2, \cdots, N)$ are the nodes in the domain of influence.

The Eq. (11) can be rewritten as the following form:

$$J = (Sa - u)^T W(z)(Sa - u) \tag{12}$$

where

$$u^T = (u_1, u_2, \cdots, u_N) \tag{13}$$

$$S = \begin{bmatrix} S_1(z_1) & S_2(z_1) & \cdots & S_M(z_1) \\ S_1(z_2) & S_2(z_2) & \cdots & S_M(z_2) \\ \vdots & \vdots & \ddots & \vdots \\ S_1(z_N) & S_2(z_N) & \cdots & S_M(z_N) \end{bmatrix} \tag{14}$$

$$W(x) = \begin{bmatrix} w(z - z_1) & 0 & \cdots & 0 \\ 0 & w(z - z_2) & \cdots & 0 \\ \vdots & \vdots & \ddots & \vdots \\ 0 & 0 & \cdots & w(z - z_N) \end{bmatrix} \tag{15}$$

Let J take the minimum, that is

$$\frac{\partial J}{\partial a} = 0 \tag{16}$$

The following form can be obtained

$$A(z)a(z) = B(z)u \tag{17}$$

where

$$A(z) = S^T W(z)S \tag{18}$$

$$B(z) = S^T W(z) \tag{19}$$

The Eq. (17) can be given as

$$a(z) = A^{-1}(z)B(z)u \tag{20}$$

Substituting Eq. (20) into Eq. (7), the approximating function $u^h(z)$ is obtained

$$u^h(z) = \Phi(z)u = \sum_{K=1}^{N} \Phi_K(z)u_K \tag{21}$$

in which shaped function $\Phi(z)$ is expressed as

$$\Phi(z) = (\Phi_1(z), \Phi_2(z), \cdots, \Phi_N(z)) = S^T(z)A^{-1}(z)B(z) \tag{22}$$

3 Governing Equation of the THCP for Meshfree RRKPM

3.1 Fundamental Equations for the THCP

From the theory of transient heat conduction, the differential equation of THCP in orthotropic plane can be expressed as

$$\frac{\partial}{\partial x}\left(k_x \frac{\partial T(z,t)}{\partial x}\right) + \frac{\partial}{\partial y}\left(k_y \frac{\partial T(z,t)}{\partial y}\right) + q_v = \rho c_p \frac{\partial T(z,t)}{\partial t} \tag{23}$$

where $T(z,t)$ represents transient temperature, t denotes transient heat transfer time, k_x and k_y represent thermal conductivities of material in plane principal axes, ρ represents density of material, c_p represents constant pressure specific heat and q_v is internal heat source intensity.

The material is assumed to be isotropic with $k_x = k_y = k$, Eq. (23) can be simplified as

$$k\left(\frac{\partial^2 T(z,t)}{\partial x^2} + \frac{\partial^2 T(z,t)}{\partial y^2}\right) + q_v = \rho c_p \frac{\partial T(z,t)}{\partial t} \tag{24}$$

or

$$\nabla^2 T(z,t) + q_v/k = (1/\alpha T)\partial T(z,t)/\partial t \tag{25}$$

in which $\alpha_T = k/\rho c_p$ represents thermal diffusivity, ∇^2 denotes Laplace operator.

$$\nabla^2 = \partial^2/\partial x^2 + \partial^2/\partial y^2 \tag{26}$$

Assuming no heat source, the Eq. (25) is rewritten as the Fourier equation:

$$\nabla^2 T = (1/\alpha_T)\partial T(z,t)/\partial t \tag{27}$$

In order to obtain the unique solution of the THCP, boundary conditions and initial conditions must be applied. There are three kinds of boundary conditions as follows:

(1) The first kind of boundary condition is that the temperature on the boundary is known, and the formula is

$$T(z,t)|_{\Gamma_1} = \bar{T}(z,t) \tag{28}$$

or

$$T(x,y,t)|_{\Gamma_1} = f(x,\ y,\ t) \tag{29}$$

in which Γ_1 represents the boundary of first kind, $\bar{T}(z,t)$ represents known boundary temperature (constant), $f(x,\ y,\ t)$ represents known boundary temperature function which changes with time.

(2) The second kind of boundary condition is that the heat flux density on the boundary is known. Because the direction of the heat flux is the exterior normal direction of the boundary, the formula is as following:

$$-(\partial T(z,t)/\partial n)|_{\Gamma_2} = \bar{h} \tag{30}$$

or

$$-(\partial T(x,y,t)/\partial n)|_{\Gamma_2} = h(x,\ y,\ t) \tag{31}$$

where Γ_2 represents the boundary of second kind of boundary condition, $\bar{h}$ represents known heat flux (constants), $h(x, y, t)$ represents known heat flux function which changes with time.

    (3) The third kind of boundary condition is that the convection or radiant heat transfer on the boundary is known. For convection heat transfer conditions

$$-k(\partial T(z,t)/\partial n)|_{\Gamma_3} = g(T(z,t) - T_q(z,t))|_{\Gamma_3} \tag{32}$$

where Γ_3 represents the boundary of third kind of boundary conditions, T represents temperature of fluid medium, g represents heat transfer coefficient.

    For radiant heat transfer conditions, it can be written as

$$-k(\partial T(z,t)\partial n)|_{\Gamma_3} = \varepsilon f \sigma_0(T^4(z,t) - T_r^4(z,t))|_{\Gamma_3} \tag{33}$$

with ε representing blackness coefficient, f denoting shaped factor, σ_0 being Stefan-Bolzman constant and $T_r(z,t)$ representing temperature of radiant source.

    The initial condition is the known value of the temperature at the beginning of the heat transfer process, and the formula is

$$T(z,t)|_{t=0} = 0 \tag{34}$$

or

$$T(z,t)|_{t=0} = T_0(x, y) \tag{35}$$

    From the heat conduction equation and boundary conditions, it can be seen that there is only one partial differential equation (PDE) and only one temperature as an unknown variable, therefore, the THCP is actually solving the PDE.

3.2 Integral Weak Form of the THCP

    In a certain instantaneous state, $T(z,t)$ and $\frac{\partial T(z,t)}{\partial t}$ can be considered as deterministic functions of plane coordinates. The THCP can be transformed to the elliptic equation of boundary value problem, and the formula is

$$\Pi = \int_{\Omega}\left[T(z,t)\left(\rho c\frac{\partial T(z,t)}{\partial t} - q_v\right)\right]d\Omega + \int_{\Omega}\left[\frac{1}{2}k_1\left(\frac{\partial T(z,t)}{\partial x}\right)^2 + \frac{1}{2}k_2\left(\frac{\partial T(z,t)}{\partial y}\right)^2\right]d\Omega$$
$$+ \int_{\Gamma_2}T(z,t)\cdot\bar{q}d\Gamma + \int_{\Gamma_3}h\left(\frac{T^2(z,t)}{2} - T(z,t)\cdot T_\alpha(z,t)\right)d\Gamma \tag{36}$$

    The field function, which makes the variational of the function Π equal zero, is the solution which satisfies the governing differential Eq. (23) and boundary condition of this problem.

    Taking the first kind of boundary problem as an example, the temperature function $T(z,t)$ must satisfy the essential boundary condition (29), which is $T(z,t) - \bar{T}(z,t) = 0$ on the boundary Γ_1, so the function Π is conditional function. Introducing the penalty function method into the essential boundary conditions (28)–(32), and another modified function Π^* can be constructed as

$$\Pi^* = \Pi + \frac{1}{2}\int_{\Gamma_1}(T(z,t) - \bar{T}(z,t))^T \cdot \beta \cdot (T(z,t) - \bar{T}(z,t))d\Gamma \tag{37}$$

with β representing penalty factor of generally $10^3 \sim 10^5$ in the THCP. After introducing essential boundary conditions, the conditional stationary value problem of original function Π transforms into the unconditional stationary value problem of modified function Π^*. The first variation of the stationary condition for modified function Π^* equals zero.

$$\delta \Pi^* = \delta \Pi + \int_{\Gamma_1} \delta(T(z,t) - \bar{T}(z,t))^T \cdot \beta \cdot (T(z,t) - \bar{T}(z,t))d\Gamma = 0 \tag{38}$$

Substituting Eq. (36) into Eq. (38), the integral weak form of the THCP is

$$\int_{\Omega} \delta T \cdot \rho c \cdot \frac{\partial T}{\partial t} d\Omega + \int_{\Omega} \delta(LT)^T \hat{k}(LT)d\Omega - \int_{\Omega} \delta T \cdot q_v d\Omega - \int_{\Gamma_2} \delta T \cdot \bar{h}d\Gamma$$
$$- \int_{\Gamma_3} \delta T \cdot g(T_\alpha - T)d\Gamma + \int_{\Gamma_1} \delta T \cdot \beta \cdot T d\Gamma - \int_{\Gamma_1} \delta T \cdot \beta \cdot \bar{T}d\Gamma = 0 \tag{39}$$

where

$$L(\cdot) = \begin{pmatrix} \dfrac{\partial}{\partial x} \\ \dfrac{\partial}{\partial y} \end{pmatrix} (\cdot) \tag{40}$$

$$\hat{k} = \begin{bmatrix} k_1 & 0 \\ 0 & k_2 \end{bmatrix} \tag{41}$$

3.3 The Meshfree RRKPM for the THCP

The THCP is a function in space domain Ω and in time domain t, and these two domains are not coupled. Therefore, the meshfree RRKPM and finite difference method (FDM) can be used to solve the problem, that is, the THCP is solved by the meshfree RRKPM in space domain and by the FDM in time domain. Firstly, the domain Ω is discretized into a finite number of nodes, and then the temperature of any point in the domain at any time t is approximated by the node temperature $T_I(t)$ in its influence domain.

$$T(t) = T_I(z_I, t) \tag{42}$$

It should be noted that $T(z_I, t)$ of any field point z in the domain is a scalar at any time, so the temperature can be given as

$$T(z,t) = \sum_{J=1}^{N} \Phi_J(z) T_J(z, t) = \Phi(z) \cdot T(t) \tag{43}$$

in which $\Phi(z)$ represents a shaped function vector, which is just a function in the space domain.

$$T = (T_1(t), \ T_2(t), \ \cdots, \ T_N(t))^T \tag{44}$$

and

$$\frac{\partial T(z,t)}{\partial t} = \frac{\partial}{\partial t} \sum_{J=1}^{N} \Phi_J(z) \cdot T_J(t) = \sum_{J=1}^{N} \Phi_J(z) \cdot \frac{\partial T_J(t)}{\partial t} = \Phi(z) \cdot \dot{T}(t) \tag{45}$$

$$\dot{T} = \left(\frac{\partial T_1(t)}{\partial t}, \ \frac{\partial T_2(t)}{\partial t}, \ \cdots, \ \frac{\partial T_N(t)}{\partial t} \right)^T \tag{46}$$

$$LT(z,t) = \sum_{J=1}^{N} \begin{pmatrix} \dfrac{\partial}{\partial x} \\ \dfrac{\partial}{\partial y} \end{pmatrix} \cdot [\Phi_J(z) \cdot T_J(t)] = \sum_{J=1}^{N} B_J(z) \cdot T_J(t) = B(z) \cdot T(t) \tag{47}$$

with

$$B(z) = (B_1(z), \ B_2(z), \ \cdots, \ B_N(z)) \tag{48}$$

$$B_J(z) = \begin{pmatrix} \dfrac{\partial}{\partial x} \\ \dfrac{\partial}{\partial y} \end{pmatrix} \cdot \Phi_J(z) = \begin{bmatrix} \Phi_{J,x}(z) \\ \Phi_{J,y}(z) \end{bmatrix} \tag{49}$$

Substituting Eqs. (43), (45) and (47) into Eq. (39), the following form can be obtained:

$$\int_\Omega \delta[\Phi(z)T]^T \cdot \rho c \cdot [\Phi(z)\dot{T}]d\Omega + \int_\Omega \delta(B(z)T)^T \hat{k}(B(z)T)d\Omega - \int_\Omega \delta[\Phi(z)T]^T \cdot q_v d\Omega$$

$$- \int_{\Gamma_2} \delta[\Phi(z)T]^T \cdot \bar{h}d\Gamma - \int_{\Gamma_3} \delta[\Phi(z)T]^T \cdot g \cdot T_\alpha d\Gamma + \int_{\Gamma_3} \delta[\Phi(z)T]^T \cdot g \cdot [\Phi(z)T]d\Gamma \tag{50}$$

$$+ \int_{\Gamma_1} \delta[\Phi(z)T]^T \cdot \beta \cdot [\Phi(z)T]d\Gamma - \int_{\Gamma_1} \delta[\Phi(z)T]^T \cdot \beta \cdot \bar{T}d\Gamma = 0$$

In order to solve the discrete system equations, the integral Eq. (50) is discussed separately below.

The first term of Eq. (50) is

$$\int_\Omega \delta[\Phi(z)T]^T \cdot \rho c \cdot [\Phi(z)\dot{T}]d\Omega = \delta T^T \left[\int_\Omega \Phi^T(z) \cdot \rho c \cdot \Phi(z)d\Omega \right] \cdot \dot{T} = \delta T^T \cdot C \cdot \dot{T} \tag{51}$$

where C represents heat capacity matrix, and can be expressed as

$$C = \begin{bmatrix} C_{11} & C_{12} & \cdots & C_{1N_t} \\ C_{21} & C_{22} & \cdots & C_{2N_t} \\ \vdots & \vdots & \ddots & \vdots \\ C_{N_t1} & C_{N_t2} & \cdots & C_{N_tN_t} \end{bmatrix} \tag{52}$$

$$C_{IJ} = \int_\Omega \Phi_I^T(z) \cdot \rho c \cdot \Phi_J(z)d\Omega \tag{53}$$

The second term of Eq. (50) is

$$\int_\Omega \delta(B(z)T)^T \hat{k}(B(z)T)d\Omega = \delta T^T \left[\int_\Omega B^T(z) \cdot \hat{k} \cdot B(z)d\Omega \right] \cdot T = \delta T^T \cdot K \cdot T \tag{54}$$

where $\boldsymbol{K}$ represents heat conduction matrix

$$\boldsymbol{K} = \begin{bmatrix} \boldsymbol{K}_{11} & \boldsymbol{K}_{12} & \cdots & \boldsymbol{K}_{1N_t} \\ \boldsymbol{K}_{21} & \boldsymbol{K}_{22} & \cdots & \boldsymbol{K}_{2N_t} \\ \vdots & \vdots & \ddots & \vdots \\ \boldsymbol{K}_{N_t1} & \boldsymbol{K}_{N_t2} & \cdots & \boldsymbol{K}_{N_tN_t} \end{bmatrix} \tag{55}$$

$$\boldsymbol{K}_{IJ} = \int_{\Omega} \boldsymbol{B}_I(z) \cdot \tilde{k}_{IJ} \cdot \boldsymbol{B}_J(z) d\Omega \tag{56}$$

The third term of Eq. (50) is

$$\int_{\Omega} \delta[\boldsymbol{\Phi}(z)\boldsymbol{T}]^T \cdot q_v d\Omega = \delta \boldsymbol{T}^T \int_{\Omega} \boldsymbol{\Phi}^T(z) \cdot q_v d\Omega = \delta \boldsymbol{T}^T \cdot \boldsymbol{F}^{(1)} \tag{57}$$

$$\boldsymbol{F}^{(1)} = (\boldsymbol{f}_1^{(1)}, \boldsymbol{f}_2^{(1)}, \cdots, \boldsymbol{f}_{N_t}^{(1)})^T \tag{58}$$

$$\boldsymbol{f}_I^{(1)} = \int_{\Omega} \boldsymbol{\Phi}_I^T(z) \cdot q_v d\Omega \tag{59}$$

The fourth term of Eq. (50) is

$$\int_{\Gamma_2} \delta[\boldsymbol{\Phi}(z)\boldsymbol{T}]^T \cdot \bar{h} d\Gamma = \delta \boldsymbol{T}^T \int_{\Gamma_2} \tilde{\boldsymbol{\Phi}}^T(z) \cdot \bar{h} d\Gamma = \delta \boldsymbol{T}^T \cdot \boldsymbol{F}^{(2)} \tag{60}$$

$$\boldsymbol{F}^{(2)} = (\boldsymbol{f}_1^{(2)}, \boldsymbol{f}_2^{(2)}, \cdots, \boldsymbol{f}_{N_t}^{(2)})^T \tag{61}$$

$$\boldsymbol{f}_I^{(2)} = \int_{\Gamma_2} \boldsymbol{\Phi}_I^T(z) \cdot \bar{h} d\Gamma \tag{62}$$

The fifth term of Eq. (50) is

$$\int_{\Gamma_3} \delta[\boldsymbol{\Phi}(z)\boldsymbol{T}]^T \cdot g \cdot T_\beta d\Gamma = \delta \boldsymbol{T}^T \int_{\Gamma_3} \boldsymbol{\Phi}^T(z) \cdot g \cdot T_\beta d\Gamma = \delta \boldsymbol{T}^T \cdot \boldsymbol{F}^{(3)} \tag{63}$$

$$\boldsymbol{F}^{(3)} = (\boldsymbol{f}_1^{(3)}, \boldsymbol{f}_2^{(3)}, \cdots, \boldsymbol{f}_{N_t}^{(3)})^T \tag{64}$$

$$\boldsymbol{f}_I^{(3)} = \int_{\Gamma_3} \boldsymbol{\Phi}_I^T(z) \cdot g \cdot T_\beta d\Gamma \tag{65}$$

where $\boldsymbol{F}^{(1)}$, $\boldsymbol{F}^{(2)}$ and $\boldsymbol{F}^{(3)}$ represent thermal load vectors known as heat source, given heat flow and heat exchange, respectively.

The sixth term of Eq. (50) is

$$\int_{\Gamma_3} \delta[\boldsymbol{\Phi}(z)\boldsymbol{T}]^T \cdot g \cdot [\boldsymbol{\Phi}(z)\boldsymbol{T}] d\Gamma = \delta \boldsymbol{T}^T \int_{\Gamma_3} \boldsymbol{\Phi}^T(z) \cdot g \cdot \boldsymbol{\Phi}(z) d\Gamma \cdot \boldsymbol{T} = \delta \boldsymbol{T}^T \cdot \boldsymbol{G} \cdot \boldsymbol{T} \tag{66}$$

where

$$G = \begin{bmatrix} G_{11} & G_{12} & \cdots & G_{1N_t} \\ G_{21} & G_{22} & \cdots & G_{2N_t} \\ \vdots & \vdots & \ddots & \vdots \\ G_{N_t1} & G_{N_t2} & \cdots & G_{N_tN_t} \end{bmatrix} \tag{67}$$

$$G_{IJ} = \int_{\Gamma_3} \Phi_I(z) \cdot g \cdot \Phi_J(z) d\Gamma \tag{68}$$

The seventh term of Eq. (50) is

$$\int_{\Gamma_1} \delta[\Phi(z)T]^T \cdot \beta \cdot [\Phi(z)T] d\Gamma = \delta T^T \int_{\Gamma_1} \Phi^T(z) \cdot \beta \cdot \Phi(z) d\Gamma \cdot T = \delta T^T \cdot K^\beta \cdot T \tag{69}$$

where

$$K^\beta = \begin{bmatrix} K^\beta_{11} & K^\beta_{12} & \cdots & K^\beta_{1N_t} \\ K^\beta_{21} & K^\beta_{22} & \cdots & K^\beta_{2N_t} \\ \vdots & \vdots & \ddots & \vdots \\ K^\beta_{N_t1} & K^\beta_{N_t2} & \cdots & K^\beta_{N_tN_t} \end{bmatrix} \tag{70}$$

$$K^\beta_{IJ} = \int_{\Gamma_1} \Phi_I(z) \cdot \beta \cdot \Phi_J(z) d\Gamma \tag{71}$$

The eighth term of Eq. (50) is

$$\int_{\Gamma_1} \delta[\Phi(z)T]^T \cdot \beta \cdot \bar{T} d\Gamma = \delta T^T \int_{\Gamma_1} \Phi^T(z) \cdot \beta \cdot \bar{T} d\Gamma = \delta T^T \cdot F^\beta \tag{72}$$

where
$$F^\beta = (f_1^\beta, f_2^\beta, \cdots, f_{N_t}^\beta)^T \tag{73}$$

$$f_I^\beta = \int_{\Gamma_1} \Phi_I^T(z) \cdot \beta \cdot \bar{T} d\Gamma \tag{74}$$

Substituting Eqs. (51), (54), (57), (60), (63), (66), (69) and (72) into Eq. (50), and the following form can be given:

$$\delta T^T (C\dot{T} + KT + GT + K^\beta T - F^{(1)} - F^{(2)} - F^{(3)} - F^\beta) = 0 \tag{75}$$

From the arbitrariness of δT^T, the final ordinary differential equations (ODE) can be given as

$$C\dot{T} + \hat{K}T - \hat{F} = 0 \tag{76}$$

where

$$\hat{K} = K + H + K^\beta \tag{77}$$

$$\hat{F} = F^{(1)} + F^{(2)} + F^{(3)} + F^{\beta} \tag{78}$$

The PDE problems of the THCP have been discretized into initial value problems of the ODE with nodal temperature $T(t)$ in space domain Ω.

The above is the meshfree RRKPM for the THCP.

4 Time Integral Scheme

Eq. (76) is the linear ODE with time t being independent variable. In order to discretize the time domain of the ODE, the traditional two-point difference method is used in this paper.

In space domain Ω, the temperature vector T is a function of time t, and can be divided into several elements. In any element, $T(z, t)$ is given as

$$T(z, t) \approx \bar{T}(z, t) = \sum N_i(z) T_i(t) \tag{79}$$

where $T_i(t) = T(t_i)$ represents nodal temperature vector at time t_i. The interpolating function $N_i(z)$ takes as same form for each component of the vector $T(z, t)$.

When the ODE only contains the first-order derivative of time t, the interpolate function is a linear polynomial, and the two-point first-order interpolation can be used.

For the time interval Δt, $T(z, t)$ can be obtained by interpolation of node values $T_n(t)$ and $T_{n+1}(t)$ in an interval

$$T(z, t) = N_n(z) T_n(t) + N_{n+1}(z) T_{n+1}(t) \tag{80}$$

The first-order derivative of $T(z, t)$ is

$$\dot{T}(z, t) = \dot{N}_n(z) T_n(t) + \dot{N}_{n+1}(z) T_{n+1}(t) \tag{81}$$

The interpolate function and the first-order derivative can be expressed by the local variable λ

$$\begin{cases} \lambda = \dfrac{t}{\Delta t} \quad (0 \le \lambda \le 1) \\ N_n = 1 - \lambda, \quad \dot{N}_n = -\dfrac{1}{\Delta t} \\ N_{n+1} = \lambda, \quad \dot{N}_{n+1} = \dfrac{1}{\Delta t} \end{cases} \tag{82}$$

Using approximating interpolation of Eqs. (80) and (81), the Eq. (76) inevitably produces residual in a time interval Δt. A weighted residual expression is derived as

$$\int_0^1 w[C(\dot{N}_n T_n + \dot{N}_{n+1} T_{n+1}) + \hat{K}(N_n T_n + N_{n+1} T_{n+1}) - \hat{F}] d\lambda = 0 \tag{83}$$

Substituting Eq. (82) into Eq. (83), the residual relation of two time intervals can be given as

$$\left(\hat{K} \int_0^1 w\lambda d\lambda + C \int_0^1 w \frac{1}{\Delta t} d\lambda \right) T_{n+1} + \left(\hat{K} \int_0^1 w(1 - \lambda) d\lambda - C \int_0^1 w \frac{1}{\Delta t} d\lambda \right) T_n - \int_0^1 w\hat{F} d\lambda = 0 \tag{84}$$

Eq. (84) can be seen as a general form applicable to any weighted function.

$$\left(\frac{C}{\Delta t} + \hat{K}\zeta \right) T_{n+1} + \left[-\frac{C}{\Delta t} + \hat{K}(1-\zeta) \right] T_n = \bar{F} \tag{85}$$

$\bar{F}$ is supposed to use the same interpolation as the unknown temperature function $T(z, t)$.

$$\bar{F} = \hat{F}_{n+1}\zeta + \hat{F}_n(1-\zeta) \tag{86}$$

Substituting Eq. (86) into Eq. (85), the following form can be expressed

$$\left(\frac{C}{\Delta t} + \zeta\hat{K}_{n+1} \right) T_{n+1} = \left(\frac{C}{\Delta t} - (1-\zeta)\hat{K}_n \right) T_n + \zeta\hat{F}_{n+1} + (1-\zeta)\hat{F}_n \tag{87}$$

here

$$\zeta = \frac{\int_0^1 w\lambda d\lambda}{\int_0^1 w d\lambda} \tag{88}$$

The above is the time difference scheme for the THCP.

5 Numerical Examples

5.1 Transient Temperature Field of the THCP in Rectangular Domain

The governing equation of the THCP in the rectangular domain is

$$\frac{\partial T}{\partial t} - \frac{\partial^2 T}{\partial x^2} - \frac{\partial^2 T}{\partial y^2} = (1+t^2)T + (2\pi^2 - t^2 - 2)e^{-t}\sin(\pi x)\cos(\pi y), \; (x, y) \in (0, 1) \tag{89}$$

According to the boundary conditions, written as

$$T(x, y, t)|_{x=0} = T(x, y, t)|_{x=1} = 0 \tag{90}$$

$$T(x, y, t)|_{y=0} = T(x, y, t)|_{y=1} = e^{-t}\sin(\pi x) \tag{91}$$

and the initial condition, given by

$$T(x, y, t)|_{t=0} = \sin(\pi x)\cos(\pi y) \tag{92}$$

The analytical solution of the THCP can be obtained as

$$T(x, y, t) = e^{-t}\sin(\pi x)\cos(\pi y) \tag{93}$$

As shown in Fig. 1, 11×11 nodes are uniformly distributed in the rectangular THCP domain Ω, and time interval $\Delta t = 0.001$ s. The penalty factor is taken as $\alpha = 1.0 \times 10^8$ and the scaling parameter is taken as $\delta = 2.0$. The regular quadrilateral background mesh is applied to the governing equation of THCP, and 4×4 Gauss integral scheme is used.

In order to discuss the influence of kernel functions on the calculation accuracy and stability, the kernel function is taken as the following two forms:

$$w_1(r_i) = \begin{cases} 1 - 6r_i^2 + 8r_i^3 - 3r_i^4 & r_i \leq 1 \\ 0 & r_i > 1 \end{cases} \tag{94}$$

$$w_2(r_i) = \begin{cases} 2/3 - 4r_i^2 + 4r_i^3 & r_i \leq 1/2 \\ 4/3 - 4r_i + 4r_i^2 - 4r_i^3/3 & 1/2 < r_i \leq 1 \\ 0 & r_i > 1 \end{cases} \tag{95}$$
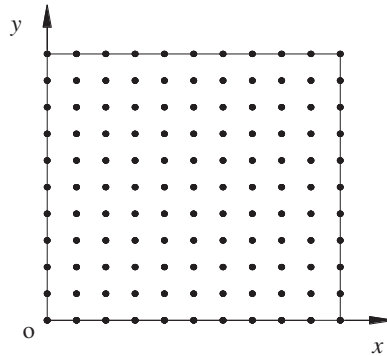
Figure 1: Distribution of nodes in rectangular domain for the THCP

In order to illustrate the validity of the proposed method, the temperature in $x = 0.5$ and at $t = 0.1$ s is calculated by the analytical solution, RKPM and RRKPM, respectively. Fig. 2 gives the comparison of the temperature between two methods using different kernel functions which the kernel function of Eq. (94) is defined as the kernel function 1 and the kernel function of (95) is defined as the kernel function 2. The relative error is defined as

$$e_{relative\ error} = \frac{|T^{analytical} - T^{numerical}|}{|T^{analytical}|} \tag{96}$$

where $T^{analytical}$ is the analytical solution and $T^{numerical}$ represents the numerical solution.
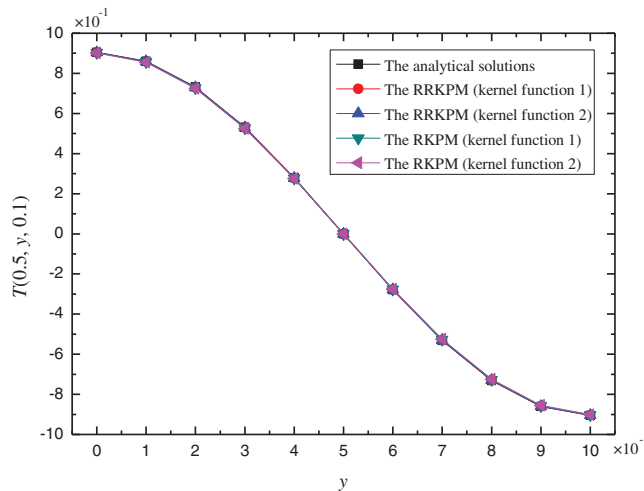
Figure 2: The temperature of the THCP for the RRKPM and the RKPM in $x = 0.5$ and at $t = 0.1$ s

Fig. 3 discusses the relative error for the RRKPM and the RKPM, and it can be found that the maximum relative errors are 0.4518% and 0.4464% for the RRKPM, and 1.8054% and 1.2586% for the RKPM, respectively. The results illustrate that the RRKPM has better accuracy and stability than that of the RKPM.
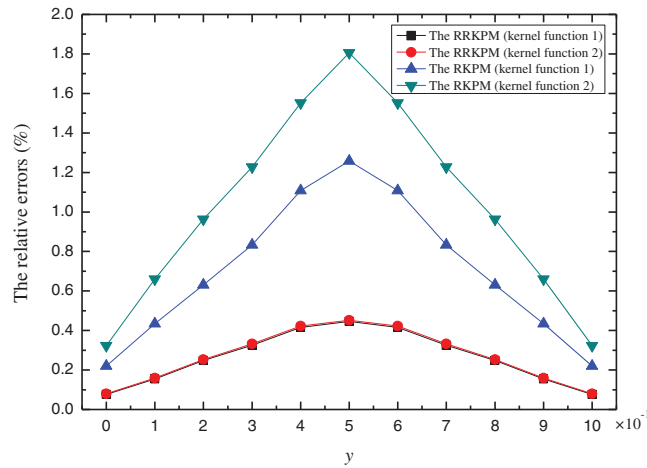
Figure 3: The relative errors of the THCP for the RRKPM and the RKPM in $x = 0.5$ and at $t = 0.1$ s

Because the kernel function 1 has better accuracy than the kernel function 2, the kernel function 1 is used in the following analysis. Fig. 4 compares the temperatures between the analytical solution and the RRKPM in $x = 0.5$ and at $t = 0.1$, 0.3, 0.5, 0.7, 0.9 s, and it can be found that the solution of RRKPM agrees well with the analytical solution.
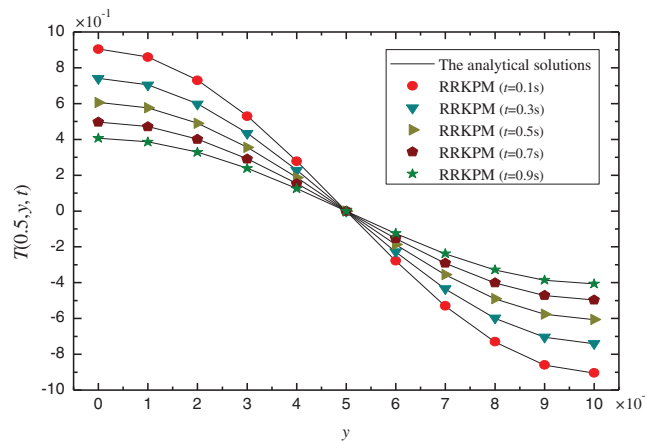
Figure 4: The temperature of the THCP for the RRKPM and the RKPM at different time in $x = 0.5$

Fig. 5 discusses the temperature among the analytical solution, the RKPM and the RRKPM in $y = 0.7$ and at $t = 0.1$ s. Fig. 6 analyzes the relative errors of the RKPM and the RRKPM. The

maximum relative errors are 0.4400% and 1.8012% for the RRKPM and the RKPM, respectively, and it can be found that the RRKPM is in better agreement with the analytical solution.
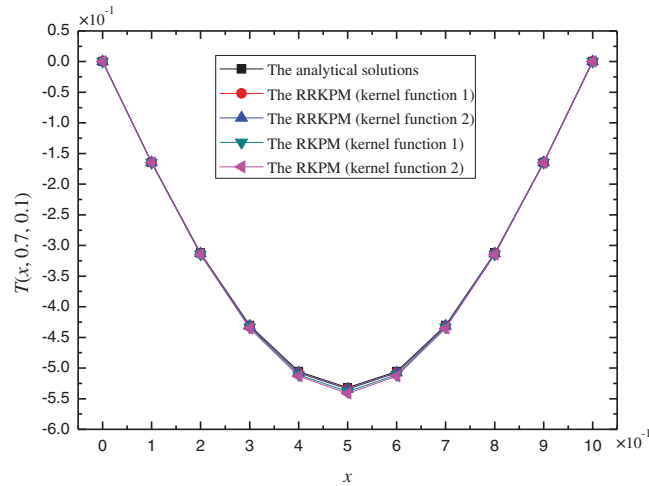
Figure 5: The temperature of the THCP for the RRKPM and the RKPM in $y = 0.7$ and at $t = 0.1$ s
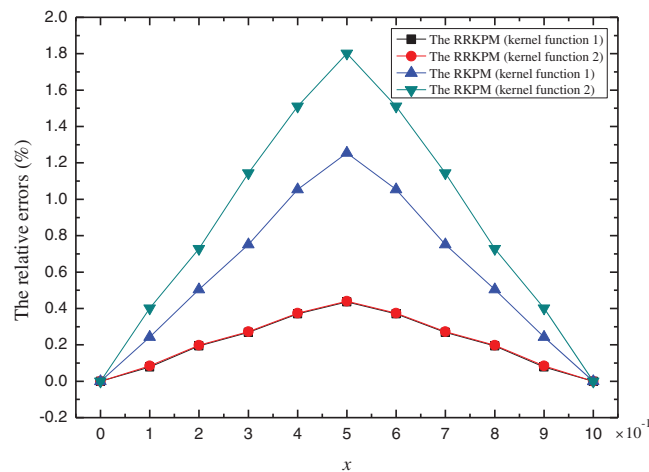
Figure 6: The relative errors between the RRKPM and the RKPM in $y = 0.7$ and at $t = 0.1$ s

Fig. 7 compares the temperature between the analytical solution and the RRKPM in $y = 0.7$ and at $t = 0.1, 0.3, 0.5, 0.7, 0.9$ s. The maximum relative error is 0.0795% for the RRKPM, and it can also be found that the RRKPM is consistent with the analytical solution.

The calculation results of the RRKPM are in better agreement with the analytical solutions, which shows that the calculation accuracy of the RRKPM is higher than that of RKPM. When different kernel functions are used for calculation, the calculated values of the RRKPM are consistent, but the RKPM has a large deviation. Meanwhile, the numerical results also show that

the calculating accuracy of the RRKPM is not affected by kernel function, and its stability is better than that of RKPM.
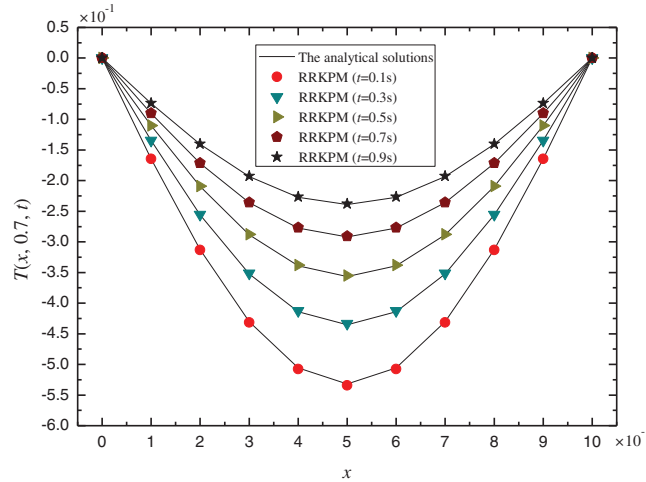
Figure 7: The temperature for the RRKPM and the RKPM in $y = 0.7$ at different time

5.2 Transient Temperature Field of the THCP in a Semi-Circular Ring Plate

The governing equation of the THCP in semi-circular ring plate is

$$\frac{\partial T(r,\theta,t)}{\partial t} - \frac{\partial^2 T(r,\theta,t)}{\partial r^2} - \frac{\partial^2 T(r,\theta,t)}{\partial \theta^2} = T(r,\theta,t), r \in [1, 2], \quad \theta \in [0, \pi] \tag{97}$$

Based on the boundary conditions

$$T(r, \theta, t)|_{r=1} = \sin\theta \cdot e^t \tag{98}$$

$$T(r, \theta, t)|_{r=2} = 0 \tag{99}$$

$$T(r, \theta, t)|_{\theta=0} = T(r, \theta, t)|_{\theta=\pi} = 0 \tag{100}$$

and the initial condition

$$T(r, \theta, t)|_{t=0} = \frac{4}{3}\left(\frac{1}{r} - \frac{r}{4}\right)\sin\theta \tag{101}$$

The analytical solution of the THCP is written as

$$T(r, \theta, t) = \frac{4}{3}\left(\frac{1}{r} - \frac{r}{4}\right)\sin\theta \cdot e^t \tag{102}$$

Fig. 8 is the node distribution in the THCP domain Ω of the semi-circular ring plate with time interval $\Delta t = 0.001$ s. The penalty factor is taken as $\alpha = 1.0 \times 10^8$ and the scaling parameter is taken as $\delta = 2.0$.
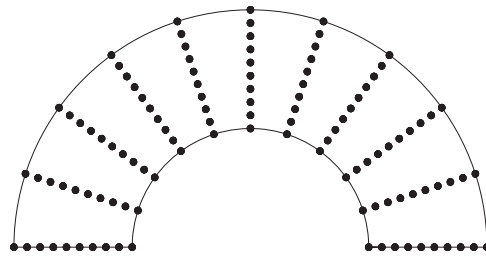
Figure 8: Node distribution in the semi-circular ring plate

The temperature in $\theta = \pi/4$ and at $t = 0.1$ s is calculated by the analytical solution, the RRKPM and the RKPM, respectively (shown as Fig. 9). In order to prove the effectiveness of the RRKPM, Fig. 10 gives the relative errors of the RRKPM and the RKPM in $\theta = \pi/4$ and at $t = 0.1$ s. It can be found from Fig. 10 that the maximum relative error is 0.4421% for the RRKPM, and 1.7556% for the RKPM. The results illustrate that the RRKPM has a higher accuracy than the RKPM.
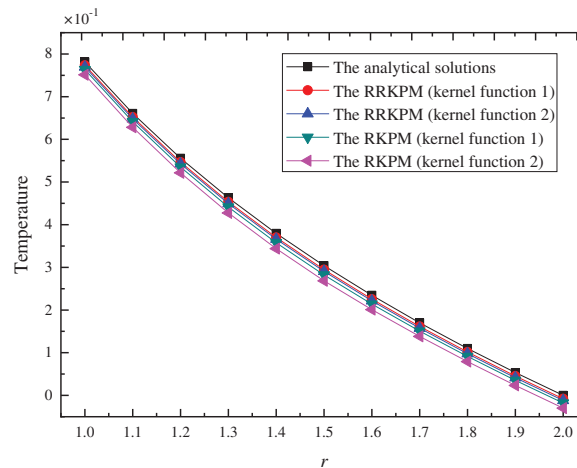
Figure 9: The temperature of the THCP for the RRKPM and the RKPM in $\theta = \pi/4$ and at $t = 0.1$ s

Fig. 11 compares the temperatures between the analytical solution and the RRKPM in $\theta = \pi/2$ and at $t = 0.1, 0.3, 0.5, 0.7, 0.9$ s. The maximum relative error is 0.4256% for the RRKPM, and it can be illustrated that the RRKPM is consistent with the analytical solution.

Fig. 12 discusses the temperature among the analytical solution, the RKPM and the RRKPM in $r = 1.8$ and at $t = 0.1$ s. Fig. 13 analyzes the relative errors of the RRKPM and the RKPM. The maximum relative error is 0.4512% for the RRKPM, and 1.8179% for the RKPM, so the RRKPM agrees well with the analytical solution.

Fig. 14 discusses the temperature among the analytical solution, the RKPM and the RRKPM in $r = 1.5$ and at $t = 0.1, 0.3, 0.5, 0.7, 0.9$ s. The maximum relative error is 0.4186% for the RRKPM, and 1.7241% for the RKPM. It can be illustrated that the solution of RRKPM is consistent with the analytical solution.
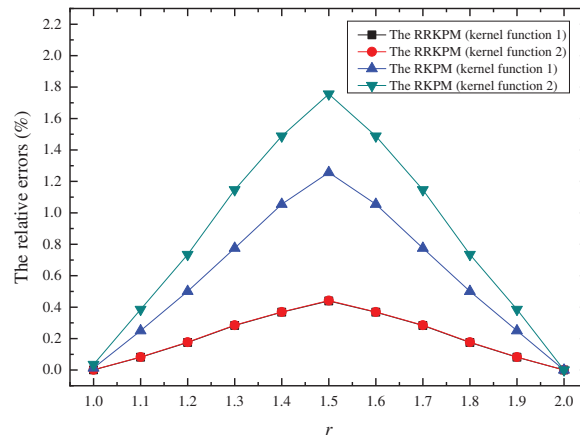
Figure 10: The relative errors of the RRKPM and the RKPM for the THCP in $\theta = \pi/4$ and at $t = 0.1$ s
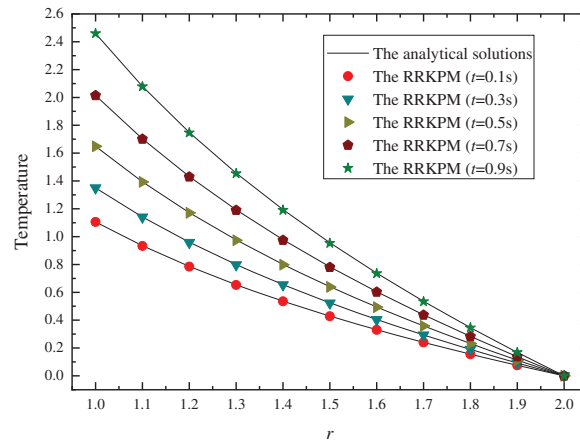
Figure 11: The temperature of the THCP for the RRKPM in $\theta = \pi/2$ at different time
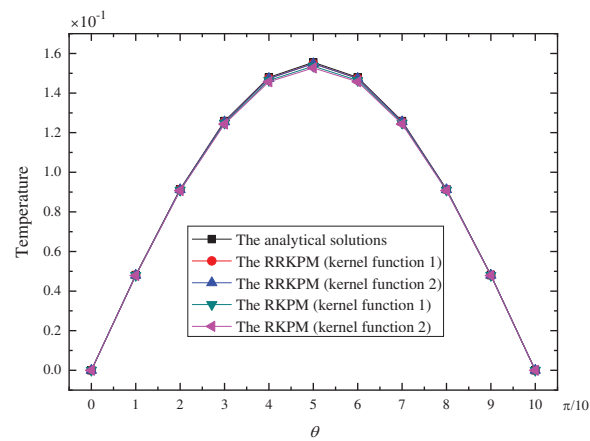
Figure 12: The temperature of the THCP for the RRKPM and the RKPM in $r = 1.8$ and at $t = 0.1$ s
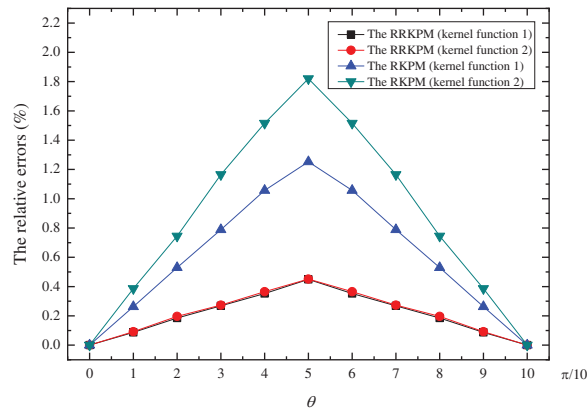
Figure 13: The relative errors of the THCP for the RRKPM and the RKPM
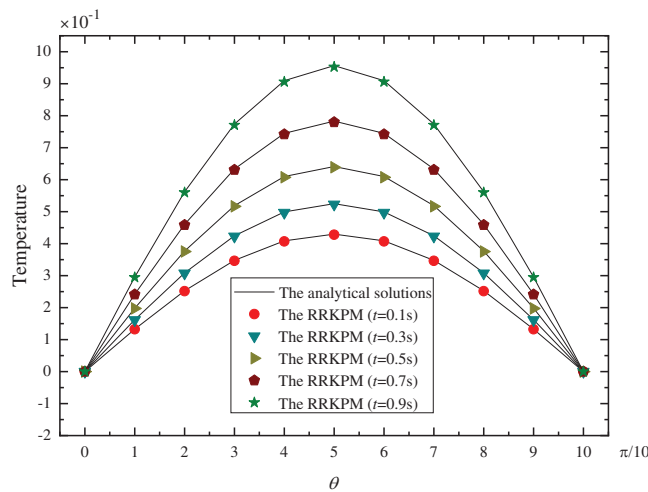
Figure 14: The temperature of the THCP for the RRKPM and the RKPM in $r = 1.5$ under different time

From above calculations, it can be shown that the calculation accuracy of the meshfree RRKPM is higher than that of the RKPM. When different kernel functions are used for calculation, the calculated values of the meshfree RRKPM are consistent, but the RKPM has a large deviation. So the numerical result of the meshfree RRKPM cannot be affected by the kernel function, and its stability is better than that of the RKPM.

6 Conclusions

A novel meshfree analysis of the RRKPM is developed for the THCP in this paper. The discrete governing equation of the THCP is established by the Galerkin weak form, and the corresponding equations of the meshfree RRKPM for the THCP are derived. From several examples of the THCP, it can be found that the meshfree analysis of the RRKPM has better calculating accuracy and convergence than that of the RKPM for solving the THCP. Meanwhile, the meshfree RRKPM can also be applied to many other interesting problems, such as complex structure dynamics, crack propagation and fracture, etc. These problems need to be further researched in the future work.

Conflicts of Interest: The authors declare that they have no conflicts of interest to report regarding the present study.

References

1. Gao, H. F., Wei, G. F. (2019). Numerical solution of potential problems using radial basis reproducing kernel particle. *Results in Physics, 13,* 102122. DOI 10.1016/j.rinp.2019.02.058.
2. Ren, H. P., Cheng, Y. M., Zhang, W. (2009). An improved boundary element-free method (IBEFM) for two-dimensional potential problems. *Chinese Physics B, 18(10),* 4065–4073. DOI 10.1088/1674-1056/18/10/002.
3. Peng, M. J., Cheng, Y. M. (2009). A boundary element-free Galerkin (BEFG) for two-dimensional potential problems. *Engineering Analysis with Boundary Elements, 33,* 77–82. DOI 10.1016/j.enganabound.2008.03.005.
4. Mirzajani, M., Khaji, N., Hori, M. (2018). Stress wave propagation analysis in one-dimensional micropolar rods with variable cross-section using micropolar wave finite element method. *International Journal of Applied Mechanics, 10(4),* 1850039. DOI 10.1142/S1758825118500394.
5. Kim, J., Dargush, G. F., Roh, H., Ryu, J., Kim, D. (2017). Unified space–time finite element methods for dissipative continua dynamics. *International Journal of Applied Mechanics, 9(2),* 1750019. DOI 10.1142/S1758825117500193.
6. Liu, M. B., Liu, G. R. (2006). Restoring particle consistency in smoothed particle hydrodynamics. *Applied Numerical Mathematics, 56,* 19–36. DOI 10.1016/j.apnum.2005.02.012.
7. Huang, R., Zheng, S. J., Liu, Z. S., Ng, T. Y. (2020). Recent advances of the constitutive models of smart materials-hydrogels and shape memory polymers. *International Journal of Applied Mechanics, 12(2),* 2050014. DOI 10.1142/S1758825120500143.
8. Liu, F. B., Wu, Q., Cheng, Y. M. (2019). A meshfree method based on the nonsingular weight functions for elastoplastic large deformation problems. *International Journal of Applied Mechanics, 11(1),* 1950006. DOI 10.1142/S1758825119500066.
9. Liu, Z., Wei, G. F., Qin, S. P., Wang, Z. M. (2022). The elastoplastic analysis of functionally graded materials using a meshfree RRKPM. *Applied Mathematics and Computation, 413,* 126651. DOI 10.1016/j.amc.2021.126651.
10. Gao, H. F., Wei, G. F. (2017). Complex variable meshfree manifold method for transient heat conduction problems. *International Journal of Applied Mechanics, 9(5),* 1750067. DOI 10.1142/S1758825117500673.
11. Gao, H. F., Cheng, Y. M. (2009). Complex variable numerical manifold method for elasticity. *Acta Mechanica Sinica (Chinese), 41(4),* 480–488.
12. Gao, H. F., Wei, G. F. (2014). Stress intensity factor for interface cracks in bimaterials using complex variable meshless manifold method. *Mathematical Problems in Engineering, 2014,* 353472. DOI 10.1155/2014/353472.

13. Peixoto, R. G., Penna, S. S., Pitangueira, R. L. S., Ribeiro, G. O. (2019). A non-local damage approach for the boundary element method. *Applied Mathematical Modelling, 69,* 63–76. DOI 10.1016/j.apm.2018.11.053.

14. Duan, W. Y., Liu, R. Z., Chen, J. K., Ma, S. (2020). Hydrodynamic analysis of floating breakwater with perforated structure based on the Taylor expansion boundary element method. *Ocean Engineering, 200,* 107044. DOI 10.1016/j.oceaneng.2020.107044.

15. Cheng, J. (2021). Residential land leasing and price under public land ownership. *Journal of Urban Planning and Development, 147(2),* 05021009. DOI 10.1061/(ASCE)UP.1943-5444.0000701.

16. Cheng, J. (2021). Analysis of commercial land leasing of the district governments of Beijing in China. *Land Use Policy, 100,* 104881. DOI 10.1016/j.landusepol.2020.104881.

17. Cheng, J. (2021). Mathematical models and data analysis of residential land leasing behavior of district governments of Beijing in China. *Mathematics, 9,* 2314. DOI 10.3390/math9182314.

18. Liu, M. B., Liu, G. R. (2010). Smoothed particle hydrodynamics (SPH): An overview and recent developments arch. *Archives Computational Methods in Engineering, 17,* 25–76. DOI 10.1007/s11831-010-9040-7.

19. Liu, M. B., Zhang, Z. L., Feng, D. L. (2017). A Density-adaptive SPH method with kernel gradient correction for modeling explosive welding. *Computational Mechanics, 4,* 1–17. DOI 10.1007/s00466-017-1420-5.

20. Cheng, Y. M., Bai, F. N., Peng, M. J. (2014). A novel interpolating element-free Galerkin (IEFG) method for two-dimensional elastoplasticity. *Applied Mathematical Modelling, 38,* 5187–5197. DOI 10.1016/j.apm.2014.04.008.

21. Cheng, Y. M., Bai, F. N., Liu, C., Peng, M. J. (2016). Analyzing nonlinear large deformation with an improved element-free Galerkin method via the interpolating moving least-squares method. *International Journal of Computational Materials Science and Engineering, 5,* 1650023. DOI 10.1142/S2047684116500238.

22. Liu, Y. H., Chen, J., Yu, S., Li, C. X. (2008). Numerical simulation of three-dimensional bulk forming processes by the element-free Galerkin method. *International Journal of Advanced Manufacturing Technology, 36(5–6),* 442–450. DOI 10.1007/s00170-006-0865-z.

23. Zheng, G. D., Cheng, Y. M. (2020). The improved element-free Galerkin method for diffusional drug release problems. *International Journal of Applied Mechanics, 12(8),* 2050096. DOI 10.1142/S1758825120500969.

24. Chen, L., Liu, C., Ma, H. P., Cheng, Y. M. (2014). An interpolating local Petrov–Galerkin method for potential problems. *International Journal of Applied Mechanics, 6(1),* 1450009. DOI 10.1142/S1758825114500094.

25. Dai, B. D., Zheng, B. J., Liang, Q. X., Wang, L. H. (2013). Numerical solution of transient heat conduction problems using improved meshfree local Petrov-Galerkin method. *Applied Mathematics and Computation, 219,* 10044–10052. DOI 10.1016/j.amc.2013.04.024.

26. Wu, Q., Peng, P. P., Cheng, Y. M. (2021). The interpolating element-free Galerkin method for elastic large deformation problems. *Science China Technological Sciences, 64,* 364–374. DOI 10.1007/s11431-019-1583-y.

27. Liu, M. B., Xie, W. P., Liu, G. R. (2005). Modeling incompressible flows using a finite particle method. *Applied Mathematical Modelling, 29,* 1252–1270. DOI 10.1016/j.apm.2005.05.003.

28. Chen, L., Cheng, Y. M., Ma, H. P. (2010). The complex variable reproducing kernel particle method for the analysis of Kirchhoff plates. *Computational Mechanics, 55,* 591–602. DOI 10.1007/s00466-015-1125-6.

29. Liu, W. K., Jun, S., Li, S., Adee, J., Belytschko, T. (1995). Reproducing kernel particle methods for structural dynamics. *International Journal of Numerical Methods for Engineering, 38,* 1655–1679. DOI 10.1002/(ISSN)1097-0207.

30. Liu, W. K., Li, S., Belytschko, T. (1997). Moving least square reproducing kernel method. (I) Methodology and convergence. *Computer Methods in Applied Mechanics and Engineering, 143,* 113–154. DOI 10.1016/S0045-7825(96)01132-2.

31. Žilinskas, A. (2010). On similarities between two models of global optimization: Statistical models and radial basis functions. *Journal of Global Optimization, 48,* 173–182. DOI 10.1007/s10898-009-9517-9.

32. Lin, S. B., Liu, X., Rong, Y. H., Xu, Z. B. (2014). Almost optimal estimates for approximation and learning by radial basis function networks. *Machine Learning, 95,* 147–164. DOI 10.1007/s10994-013-5406-z.

33. Gao, H. F., Cheng, Y. M. (2010). A complex variable meshfree manifold method for fracture problems. *International Journal of Computational Methods, 7(1),* 55–81. DOI 10.1142/S0219876210002064.

34. Huang, Z. Y., Yang, X. (2011). Tailored finite point method for first order wave equation. *Journal of Scientific Computing, 49,* 351–366. DOI 10.1007/s10915-011-9468-4.

35. Tatari, M., Kamranian, M., Dehghan, M. (2011). The finite point method for the p-Laplace equation. *Computational Mechanics, 48,* 689–697. DOI 10.1007/s00466-011-0613-6.

36. Cui, X. Y., Liu, G. R., Li, G. Y. (2011). A smoothed Hermite radial point interpolation method for thin plate analysis. *Archive of Applied Mechanics, 81,* 1–18. DOI 10.1007/s00419-009-0392-0.

37. Liu, Y., Hon, Y. C., Liew, K. M. (2006). A meshfree Hermite-type radial point interpolation method for Kirchhoff plate problems. *International Journal for Numerical Methods in Engineering, 66,* 1153–1178. DOI 10.1002/(ISSN)1097-0207.

38. Rocca, A. L., Power, H. (2006). A hermite radial basis function collocation approach for the numerical simulation of crystallization processes in a channel. *Communications Numerical Methods Engineering, 22,* 119–135. DOI 10.1002/cnm.801.

39. Ma, J. C., Wei, G. F., Liu, D. D., Liu, G. T. (2017). The numerical analysis of piezoelectric ceramics based on the Hermite-type RPIM. *Applied Mathematics and Computation, 309,* 170–182. DOI 10.1016/j.amc.2017.03.045.

40. Mantegh, I., Jenkin, M. R. M., Goldenberg, A. A. (2010). Path planning for autonomous mobile robots using the boundary integral equation method. *Journal of Intelligent & Robotic Systems, 59,* 191–220. DOI 10.1007/s10846-010-9394-y.

41. Xie, G. Z., Zhang, J. M., Huan, C., Lu, C. J., Li, G. Y. (2014). A direct traction boundary integral equation method for three-dimension crack problems in infinite and finite domains. *Computational Mechanics, 53,* 575–586. DOI 10.1007/s00466-013-0918-8.

42. Liu, Z., Wei, G. F., Wang, Z. M. (2020). Geometrically nonlinear analysis of functionally graded materials based on reproducing kernel particle method. *International Journal of Mechanics and Materials in Design, 16,* 487–502. DOI 10.1007/s10999-019-09484-8.

43. Liu, Z., Wei, G. F., Wang, Z. M. (2019). Numerical analysis of functionally graded materials using reproducing Kernel particle method. *International Journal of Applied Mechanics, 11(6),* 1950060. DOI 10.1142/S1758825119500601.

44. Qin, S. P., Wei, G. F., Liu, Z., Shen, X. H. (2021). Elastodynamic analysis of functionally graded beams and plates based on meshless RKPM. *International Journal of Applied Mechanics, 13(4),* 2150043. DOI 10.1142/S1758825121500435.

45. Young, D. L., Chen, K. H., Lee, C. W. (2005). Novel meshless method for solving the potential problems with arbitrary domain. *Journal of Computational Physics, 209,* 290–321. DOI 10.1016/j.jcp.2005.03.007.

46. Chen, T., Raju, I. S. (2003). A coupled finite element and meshless local Petrov-Galerkin method for two-dimensional potential problems. *Computer Methods in Applied Mechanics and Engineering, 192,* 4533–4550. DOI 10.1016/S0045-7825(03)00421-3.

47. Deng, Y. J., Chao, L., Peng, M. J., Cheng, Y. M. (2015). The interpolating complex variable element-free Galerkin method for temperature field problems. *International Journal of Applied Mechanics, 7(2),* 1550017. DOI 10.1142/S1758825115500179.